Fourier spectroscopy of a spin-orbit coupled Bose gas

Ana Valdés-Curiel, Dimitri Trypogeorgos, Erin Marshall, Ian B. Spielman

Joint Quantum Institute, University of Maryland and National Institute of Standards and Technology, College Park, Maryland, 20742, USA

Abstract.

We propose a time domain technique to measure the band structure of a spin-1 spin-orbit coupled Bose-Einstein condensate that relies on the Hamiltonian evolution of the system. We drive transitions at different values of detuning from Raman resonance and extract the Fourier components of the time dependent evolution to reconstruct the spin and momentum dependent energy spectrum. We add a periodic modulation to one Raman field which results in a tunable spin-orbit coupling dispersion and a spectrum of Floquet quasi-energies that we can directly measure, showing the robustness of our technique.

1. Introduction

Spinorbit (SO) coupling is an essential mechanism for most spintronics devices and leads to many fundamental phenomena in condensed matter physics and atomic physics. For example, SO coupling gives rise to the quantum spin Hall effect in electronic condensed matter systems

Start with corny paragraph, about soc and how cold atoms are awesome. Describe SOC at high field and at four photon resonance. Describe Fourier spectroscopy. Describe modulated Raman.

1.1. Fourier spectroscopy of spin-orbit coupled atoms

The relation between the dynamics of a system and its energy spectrum is rooted in the heart of quantum mechanics.

$$\begin{aligned}\hat{H} =&\frac{\hbar^2\hat{k}^2}{2m} + \alpha_0\hat{k}\hat{F}_z + 4E_L\mathbb{I} + \frac{\Omega_R}{2}\hat{F}_x] \\ &+ (\epsilon + 4E_L)(\hat{F}_z^2 - \mathbb{I}) + \Delta_0\hat{F}_z,\end{aligned} \tag{1}$$

where we have introduced the natural units of our system: the single photon recoil momentum $k_L = \frac{2\pi}{\lambda_R}\sin(\theta/2)$ and its associated recoil energy $E_L = \frac{\hbar^2 k_L^2}{2m}$, determined by the wavelength and geometry of the Raman field. We have additionally introduced the spin-orbit coupling strength $\alpha_0 = \frac{\hbar^2 k_L}{m}$ and the Raman coupling strength $\Omega_R \propto E_A^\star E_B$ which is proportional to the field intensity.

In order to explicitly measure the energy-momentum dispersion relation, we will use a Fourier based spectroscopy technique, which relies on the time evolution of an atomic state after a dressing field is suddenly turned on, and the initially bare states become superpositions of dressed states undergoing Rabi oscillations in time with spectral components related to the relative energies of the dressed states.

For the case of a spin-orbit coupled atomic system, the dressed state energies are explicitly dependent on both the particle's spin and momentum. Therefore, in order to fully characterize the energy-momentum dispersion we must prepare an atomic state at a given spin and momentum $|k_i, m_{f_i}\rangle$, pulse on the Raman field, and measure the time evolution.

In practice it is not as straightforward to reliably prepare an arbitrary momentum state in the lab. The measurement however can be simplified by noticing that a non-moving atom cloud in the laboratory reference frame dressed by a field with non-zero detuning is equivalent to a moving cloud with a resonant field in a suitable moving reference frame. This can be explicitly seen in the Hamiltonian 1 where the detuning term δ/Er and the momentum term $4k/k_R$ have the same effect in the relative energies. There is an additional Doppler shift associated with the transformation between reference frames, which gets canceled when we look at the energy differences. Therefore, for the purpose of our experiments, momentum and detuning are equivalent up to a numerical factor.

The method described above only allows us to measure relative energies and we must add a known energy reference if we want to recover the dispersion relation. We can do so by measuring the effective mass $m^\star = \hbar^2[\frac{d^2E(k_x)}{dk_x}]^{-1}$ of the nearly quadratic lowest branch of the dispersion, and then shifting the measured frequencies accordingly.

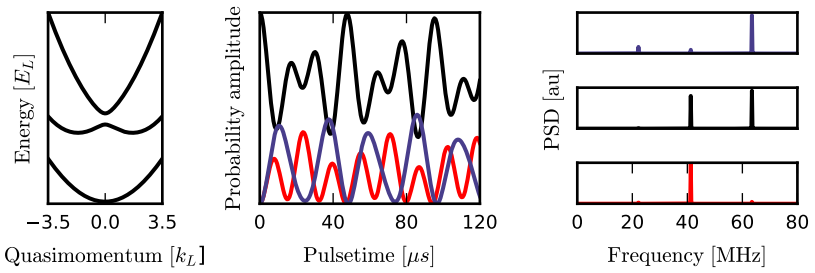

Figure 1. a) Top: Computed cross-sectional cuts of the total potential $V(y)$ (black), effective magnetic field $\mathcal{B}$ (blue) and atomic density $n(y)$ (yellow). Columns correspond to Raman coupling strengths $\hbar = 0.5, 3.5, 5.5 E_L$ respectively, all with the detuning gradient . Bottom: GPE-computed 2D density distributions $n(x, y)$ using the same parameters. **b)** Second-moment of the momentum distribution as a function of and in our system. Regions with large moments represent large potential well separations that have a synthetic magnetic field localized between the BECs.

Here an image of dispersion, time evolution, FFT, spectrum of energy differences and reconstructed spectrum.

In order to maximize our signal to noise ratio (SNR) and minimize the required number of data points we use some fancy algorithm that I'm still not sure which one will work best. We also choose the spacing and the total number of pulses for each spectra so that the bandwith and resolution of the Fourier transform allow us to resolve the frequencies of interest.

1.2. Spectroscopy of a driven system

Previous studies have shown that periodically driven systems such as cold atoms in driven optical fields[karina, optical lattices, germany group] exhibit effective coupling terms in the Hamiltonian that arise from averaging the fast dynamics of the system. Our Fourier based spectroscopy can also be used to study such systems as it can reveal additional information about the system's Floquet quasi-energy spectrum. We will focus on the case of a spin-1 spin-orbit coupled system that is coupled by a multiple frequency Raman field, as shown in Fig 3b. The interference of the multiple frequencies lead to a periodic amplitude modulation in the field and an effective Floquet Hamiltonian that has tunable spin-orbit coupling.

If we add two sidebands to one Raman beam, offset from the carrier frequency by $\pm\delta\omega$ and, for simplicity, we choose al the relative phases to be zero, then the Hamiltonian in Eq.1 remains unchanged, except for the coupling strength that takes the form $\Omega_R(t) = \Omega_0 + \Omega\cos(\delta\omega t)$. Our periodically driven system is well described by Floquet theory: the eigenstates are of the form $|\Psi(t)\rangle = \sum_j c_j e^{i\epsilon_j t}|u_j(t)\rangle$ where $|u(t)\rangle$ are time-periodic states and the ϵ_j are the Floquet quasi-energies, wich are $\epsilon_j, n = \epsilon_{j,m} + (n-m)2\pi/T$

The time evolution of the system after one driving cycle can be described in terms of an effective time-independent Hamiltonian $e^{iT\hat{H}_{eff}}$. If $\delta\omega \gg \epsilon$ and $\delta\omega \gg 4E_L$, this effective Floquet Hamiltonian retains the form of 1 with renormalized coefficients, and

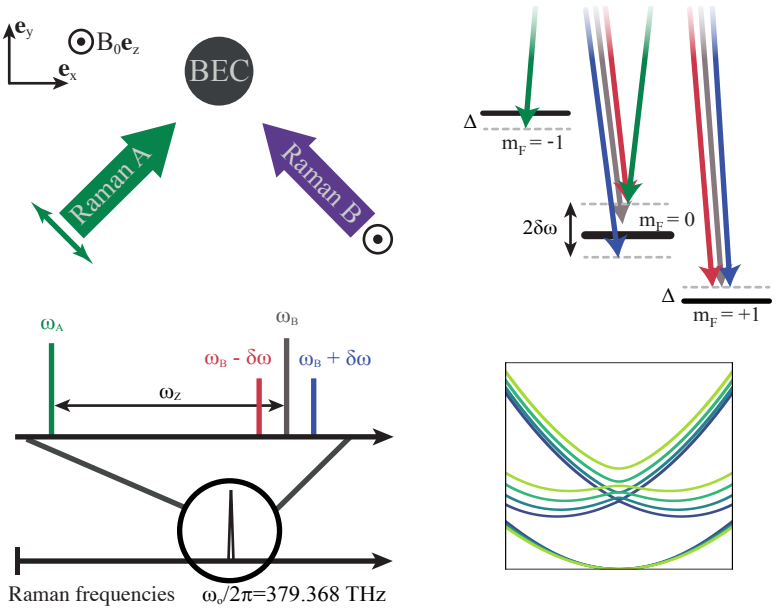

Figure 2. Time evolution of the BEC for Raman pulsing times between 5 and 10 μs, for different spin orbit coupling regimes: **(i)** $\Omega_0 = 9.9E_L$, $\Omega = 04$, $\Delta = 5.8E_L$, **(ii)** $\Omega_0 = 0$, $\Omega = 8.6E_L$, $\Delta = -0.7E_L$, and **(iii)** $\Omega_0 = 1.5E_L$, $\Omega = 8.4E_L$, $\Delta = -4.7E_L$

an additional term that explicitly couples the $m_f = -1$ and $m_f = +1$ states:

$$\begin{aligned}\hat{H} =& \frac{\hbar^2\hat{k}^2}{2m} + \alpha\hat{k}\hat{F}_z + 4E_L\mathbb{I} + \frac{\Omega_0}{2}\hat{F}_x \\ &+ \frac{\tilde{\Omega}}{2}\hat{F}_{xz} + (\tilde{\epsilon} + 4E_L)(\hat{F}_z^2 - \mathbb{I}) + \tilde{\Delta}\hat{F}_z,\end{aligned} \tag{2}$$

with $\alpha = J_0(\Omega/2\delta\omega)\alpha_0$, $\tilde{\Omega} = 1/4(\epsilon + 4E_L)(J_0(\Omega/\delta\omega) - 1)$, $\Delta = J_0(\Omega/2\delta\omega)\Delta_0$, and $\tilde{\epsilon} = 1/4(4E_L - \epsilon) - 1/4(4E_L + 3\epsilon)J_0(\Omega/\delta\omega)$

There are two limiting cases of this effective Hamiltonian 2 which will be of interest: (1) for large quadratic Zeeman shift the system can be described as an effective spin 1/2 (cite Lindsay) system where the spin orbit coupling strength and the Raman coupling can be independently tuned and

$$\hat{H}_{eff} = \frac{\hbar^2}{2m}(\hat{k} + 2k_R\hat{\sigma}_z)^2 + \frac{\hbar\Omega'}{2}\hat{\sigma}_x + \Delta\hat{\sigma}_z \tag{3}$$

where we have defined an effective coupling between the $m_f = -1$ and $m_f = +1$ states $\Omega' = \tilde{\Omega} + \hbar\Omega_0^2/2(\tilde{\epsilon})$.

Fig1b shows the high field dispersion relation, both for the modulated and unmodulated cases (here goes an image of bands). The minima, originally locted

at $\pm 2k_L$, are shifted and the size of the spin-orbit gap is changed for different choices of Ω_0, Ω, and $\delta\omega$.

2. Experiment

2.1. Spectroscopy experimental sequence

We start our experiments with a Rb^{87} Bose-Einstein condensate (BEC) with $N \approx 4 \times 10^4$ (measure) atoms in the $|F = 1, m_F = 0\rangle$ state, confined in a 1064 nm crossed optical dipole trap, with trapping frequencies $(\omega_x, \omega_y, \omega_z) = 2\pi(42(3), 34(2), 133(3))$ Hz. We break the degeneracy between the m_F magnetic sub-levels by applying a 17.0556 G bias field along the z axis, which produces a Zeeman splitting of 12 MHz and a quadratic Zeeman shift that lowers the energy of the $|F = 1, m_F = 0\rangle$ state by 20.9851 kHz. We apply a pair of microwave pulses to monitor and stabilize the bias field and. We generate spin-orbit coupling between the magnetic sub levels with a pair of intersecting, cross-polarized Raman beams, with wavelength $\lambda = 790.33nm$ propagating along $\mathbf{e}_x + \mathbf{y}$ and $\mathbf{e}_x - \mathbf{e}_y$ as shown in Fig 1a. We offset the frequency of the beams using two acusto optic modulators (AOMs), one of them driven by a superposition of up to three different frequencies. On resonance, the laser frequencies satisfy the condition $\omega_A - \omega_B = \omega_A - \frac{\omega_{B+} + \omega_{B-}}{2} = \omega_Z$, and we change the Raman detuning conditions by keeping the magnetic field constant and changing the value of the frequency ω_A.

For a given detuning value, we pulse our Raman beams for time intervals between 5 μs and up to 900 μs. We then release the atoms from the optical dipole trap and let them fall for a 21 ms time of flight (TOF) time before we image them using resonant absorption imaging. Our images reveal the atoms spin and momentum distribution, from which we can extract the full dynamics of the system.

2.2. Effective mass measurement

We measure the atom's ground state effective mass by inducing dipole oscillations in our BECs for both the bare and Raman dressed atoms. The effective mass $m^\star$ of the dressed atoms is related to the bare mass m and the bare and dressed trapping frequencies ω and ω^star by the ratio $m^\star/m = \sqrt{\omega^\star/\omega}$

To measure the trapping frequencies, we prepare our system in $|F = 1, m_F = 0\rangle$ and adiabatically turn on the Raman in ≈ 10 ms while also ramping the detuning to a non-zero value, around $0.5E_R$. Our system does not have the capability to dynamically change the laser frequency while maintaining phase stability, so unlike the pulsing experiments, we ramped the magnetic field to change the resonance conditions. This magnetic field induced detuning shifts the minima in the ground state energy away from zero quasi-momentum. We then suddenly snap the field back to resonance which changes the equilibrium conditions of the system and excites the dipole mode of our optical dipole trap. For the bare state frequency, we repeat the same procedure but we completely snap off the Raman after the initial ramp.

For this set of measurements we modified our trapping frequencies to $(\omega_x, \omega_y, \omega_z) = 2\pi(35.9, 32.5, xx)$ Hz so that they were nominally symmetric along the $x - y$ plane.

2.3. Magnetic field stabilization

We stabilized the magnetic field and measured fluctuations about the desired set point by applying a pair of microwave pulses with frequencies close to resonance from the $5^2S_{1/2}$ $F = 2$ state, and imaging the in-situ the population transfered by each pulse.

We first prepare our BEC in the $|F = 1, m_f = 0\rangle$ state and apply a 17.0556 G bias filed along the z axis. We then apply a pair of $250\mu s$ microwave pulses close to $6.83GHz$ that transfers about 10% of the atoms into the $F = 2$ manifold. The pulses were detuned by ± 2 kHz from the $|F = 1, m_F = 0\rangle \leftrightarrow |F = 2, m_F = 1\rangle$ transition and were spaced in time by 2 periods of 60 Hz. We image the atoms transfered into $F = 2$ non-destructively using absorption imaging without repumping light. The imbalance in the number of atoms transferred by each pulse gives us a 4 kHz wide error signal that we use both to feed forward our bias coils for active field stabilization, and also to keep track of the magnetic fields at each shot. We trigger our sequence to the line and both the microwave and Raman pulses are timed at integer periods of 60 Hz and performed at the zero-derivative point of the 60 Hz curve in order to minimize additional magnetic field fluctuations

3. Results

We measured the spin-orbit dispersion using our Fourier based technique for three cases: (i) $\Omega = 0$ and $\Omega_0 \neq 0$, (ii)$\Omega \neq 0$ and $\Omega_0 = 0$, and (iii)$\Omega \neq 0$ and $\Omega_0 \neq 0$.

We calibrated the Raman coupling terms Ω and Ω_0 and the detuning from Raman resonance Δ by fitting the three-level Rabi oscillations of the $m_F = 0$ and $m_f = \pm 1$ states to the time evolution given by the Hamiltonian in Eq. 1. Figure nn shows representative traces for the time evolution of our system for the three cases outlined above. It can be noted that due to the structure of the Floquet quasi-energy spectrum, the time evolution shows higher frequency components for cases (ii) and (iii). These calibrations along with the information gained from the images of atoms out-coupled with microwaves guaranteed that we were indeed at the correct detuning from Raman resonance and that the Raman coupling strength remained nominally constant throughout our measurements.

To calculate the effective mass we fitted sinusoids to the sloshing motion of our atoms in the dipole trap and extracted the frequency of oscillation. Since our Raman beams are at a 45° (can probably measure with more accuracy) angle with respect to the optical dipole trap beams, the rotation $\mathbf{e}_x + \mathbf{e}_y$ $x \to \frac{x+y}{\sqrt{2}}$, $y \to \frac{x-y}{\sqrt{2}}$ leads to a trapping frequency along the Raman recoil momentum direction $\omega = \sqrt{\omega_x^2 + \omega_y^2}$ for an axially symmetric trap. Figure $nn + 1$ shows the dipole oscillations of the Raman dressed BECs in the optical dipole trap for the three different coupling regimes as well as the bare state motion.

We use a not-uniform fast Fourier transform algorithm (NUFFT) which allows us to get the power spectral density for data points that are not necessarily evenly spaced in time as required by regular FFT algorithms. In order to account for missing data points. Figure $nn + 2$ shows the power spectral density (PSD) of the time evolution of each m_f state. Each vertical cut is normalized to the highest peak of the three spin states. We then rescale the units $\hbar\Delta \to \hbar^2 k_x/8m$, extract the highest peaks in the PSD and offset their frequency by $\hbar^2 k_x^2/2m^\star$, finally obtaining the characteristic spin- and momentum- dependent dispersion of a spin orbit coupled system. For the

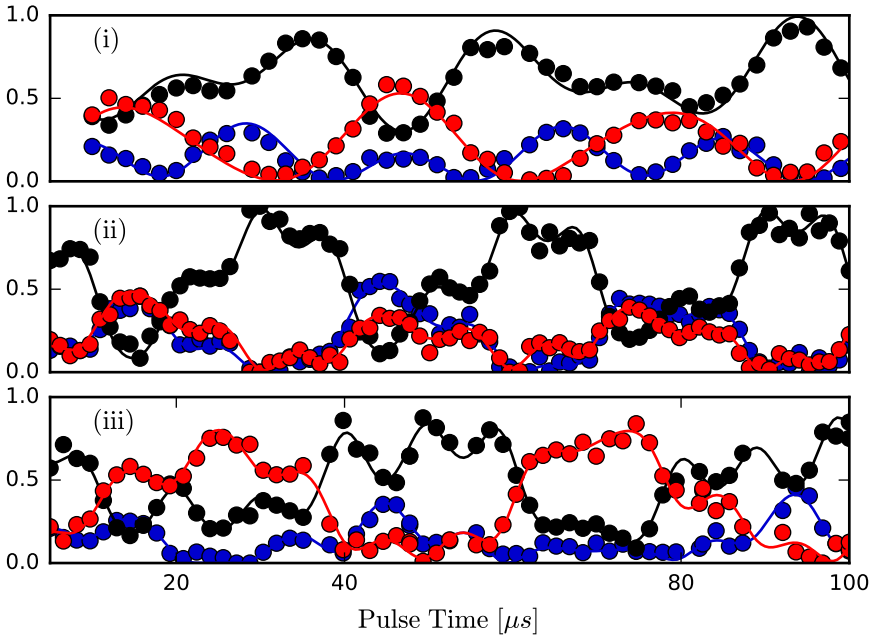

Figure 3. Time evolution of the BEC for Raman pulsing times between 5 and 10 μs, for different spin orbit coupling regimes: **(i)** $\Omega_0 = 9.9E_L$, $\Omega = 04$, $\Delta = 5.8E_L$, **(ii)** $\Omega_0 = 0$, $\Omega = 8.6E_L$, $\Delta = -0.7E_L$, and **(iii)** $\Omega_0 = 1.5E_L$, $\Omega = 8.4E_L$, $\Delta = -4.7E_L$

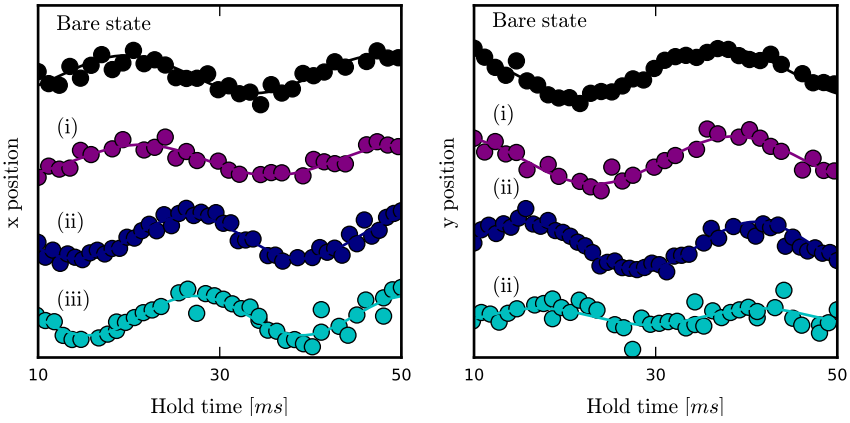

Figure 4. **a)** Top: Computed cross-sectional cuts of the total potential $V(y)$ (black), effective magnetic field $\boldsymbol{\mathcal{B}}$ (blue) and atomic density $n(y)$ (yellow). Columns correspond to Raman coupling strengths $\hbar = 0.5, 3.5, 5.5E_L$ respectively, all with the detuning gradient . Bottom: GPE-computed 2D density distributions $n(x, y)$ using the same parameters. **b)** Second-moment of the momentum distribution as a function of and in our system. Regions with large moments represent large potential well separations that have a synthetic magnetic field localized between the BECs.

case driven spin-orbit coupling (cases (ii) and (iii)), since the strength of the drive is comparable to the quadratic Zeeman shift,we observe higher frequency components in the dynamics which are in good agreement with Floquet theory.

Our system has dark states at $\Delta = 0$ which can be noted by the missing peaks in the PSD. Since there are eigenstates of the Raman dressed Hamiltonian that never get populated, the time evolution of the system does not have the frequency components related to the missing eigenstates.

4. Discussion

Spectroscopy of bloch bands?

Heating due to scattering of spontaneously emitted photons is always present in our system. It is also well known that heating is present in periodically driven systems, and while it can be minimized by increasing the driving frequency one in exchange requires more Raman power to tune the spin-orbit coupling strength. The time scales of our pulsing experiments never exceeded 1 ms which is small compared to the lifetime of our system.

In conclusion, we can measure the spin and momentum dependent dispersion relation for a spin-1 spin-orbit coupled BEC using our Fourier spectroscopy thechnique. This method is good for any (effective) three level system with a quadratic Zeeman shift $\epsilon > 4E_L$ and does not require any additional hardware as it relies only on the Hamiltonian evolution of the system. Our technique can also be useful to measure the Floquet quasi energy spectrum and the coupling within different Floquet manifolds for driven systems.

5. Conclusion

6. Appendix A

6.1. Effective SOC Hamiltonian

The effective spin-orbit coupling Hamiltonian can be derived from the electric dipole Hamiltonian describing the interaction between our Rb atoms and the multiple frequency Raman lasers

$$\hat{H}_{AL}(t) = \left[\Omega_{21}\cos(2k_R x - \omega_{21}t + \phi_1) + \Omega_{31}\cos(2k_R x - \omega_{31}t + \phi_2) + \Omega_{41}\cos(2k_R x - \omega_{41}t + \phi_3)\right]\hat{F}_x \tag{4}$$

where $\Omega_{ij} \propto \vec{E_i} \times \vec{E_j^\star}$ represents the coupling strength associated to each pair of Raman beams and $\omega_{ij} = \omega_i - \omega_j$. We choose the frequencies so that $\omega_{31} + \omega 21$ is at 4 photon resonance with the $m_f = +1 \rightarrow m_f = -1$ transition. We then apply a rotation about the z axis $\hat{U} = e^{i\bar{\omega}t\hat{F}_z}$ where $\bar{\omega} = \frac{\omega_{21}+\omega_{31}}{2}$. For the choice of parameters $\Omega_{21} = \Omega_{31} = \Omega$, $\Omega_{41} = \Omega_0$, and $\omega_{41} = \frac{\omega_{21}+\omega_{31}}{2}$,and after applying the rotating wave approximation (RWA), the Hamiltonian transforms to

$$\hat{\tilde{H}}_{AL}(t) = \frac{1}{2}\{\Omega\cos(2k_Rx + \delta\omega t + \phi_1) + \Omega\cos(2k_Rx - \delta\omega t + \phi_2) + \Omega_0\cos(2k_Rx + \phi_3)\}\hat{F}_x$$
$$- \frac{1}{2}\{\Omega\sin(2k_Rx + \delta\omega t + \phi_1) + \Omega\sin(2k_Rx - \delta\omega t + \phi_2) + \Omega_0\sin(2k_Rx + \phi_3)\}\hat{F}_y \tag{5}$$

we have the freedom of defining the time origin so we can get rid of one phase, lets make it ϕ_3 for convenience. Can I get rid of a second phase? Make $\phi_1 = -\phi_2$

$$\hat{\tilde{H}}_{AL}(t) = [\frac{\Omega_0}{2} + \Omega\cos(\delta\omega t + \phi_1)][\cos(2k_Rx)\hat{F}_x - \sin(2k_Rx)\hat{F}_y], \tag{6}$$

where we have defined $\delta\omega = \frac{\omega_{31}-\omega_{21}}{2}$. This Hamiltonian term describes a helically precessing effective Zeeman field with amplitude oscillating periodically in time.

The complete Hamiltonian can therefore be written as

$$\hat{H}(t) = \frac{\hbar^2}{2m}\hat{k}^2 + \mu\mathbf{B}_{eff}\cdot\hat{\mathbf{F}} \tag{7}$$

(check units here) with $\mu\mathbf{B}_{eff} = (\frac{\Omega_0}{2} + \Omega\cos(\delta\omega t + \phi_1))(\cos(2k_Rx)\mathbf{e}_x - \sin(2k_Rx)\mathbf{e}_y) + \Delta_0\mathbf{e}_z$

We can apply a position dependent rotation $\hat{U} = e^{i2k_Rx\hat{F}_z}$ transforms our Hamiltonian into the form of Eq. 1 with a time dependent Raman coupling.

$$\begin{aligned}\hat{H}(t) =& \frac{\hbar^2}{2m}(\hat{k} - 2k_R\hat{F}_z)^2 + (\frac{\Omega_0}{2} + \Omega\cos(\delta\omega t))\hat{F}_x \\ &+ \epsilon(\hat{F}_z^2 - \mathbb{I}) + \Delta\hat{F}_z \\ =& \frac{\hbar^2\hat{k}^2}{2m} + \alpha_0\hat{k}\hat{F}_z + 4E_L\mathbb{I} + \frac{\Omega(t)}{2}\hat{F}_x \\ &+ (\epsilon + 4E_L)(\hat{F}_z^2 - \mathbb{I}) + \Delta_0\hat{F}_z\end{aligned} \tag{8}$$

(check factors of 2!)

To get rid of the time dependence in the Hamiltonian and ultimately getting the 'tunable' spin-orbit coupling we can choose a transoformation of the Hamiltonian such that $\hat{U}^\dagger\frac{\partial\hat{U}}{\partial t} = -i\frac{\Omega(t)}{2}\hat{F}_x$. This will be satisfied for

$$\hat{U} = e^{-i\frac{\Omega}{2}\int_0^t\cos(\delta\omega t')dt'} = e^{-i\frac{\Omega}{2\delta\omega}\sin(\delta\omega t)}. \tag{9}$$

Under this time dependent transformation, the time evolution of the system will be given by the Hamiltonian

$$\begin{aligned}\hat{\tilde{H}} =& \hat{U}^\dagger\hat{H}(t)\hat{U} + i\hat{U}^\dagger\frac{\partial\hat{U}}{\partial t} \\ =& \frac{\hbar^2\hat{k}^2}{2m} + \alpha\hat{k}\hat{F}_z + 4E_L\mathbb{I} + \frac{\Omega_0}{2}\hat{F}_x \\ &+ \frac{\tilde{\Omega}}{2}\hat{F}_{xz} + (\tilde{\epsilon} + 4E_L)(\hat{F}_z^2 - \mathbb{I}) + \Delta\hat{F}_z\end{aligned} \tag{10}$$

which is exactly Eq. 2. To arrive to this final form we have transformed the operators that don't commute with $\hat{F}_x$ as

$$\begin{aligned} e^{i\theta\hat{F}_x}\hat{F}_z e^{-i\theta\hat{F}_x} &= \cos\theta\hat{F}_z + \sin\theta\hat{F}_y \\ e^{i\theta\hat{F}_x}\hat{F}_y e^{-i\theta\hat{F}_x} &= -\sin\theta\hat{F}_z + \cos\theta\hat{F}_y \\ e^{i\theta\hat{F}_x}\hat{F}_z^2 e^{-i\theta\hat{F}_x} &= \cos^2\theta\hat{F}_z^2 + \sin^2\theta\hat{F}_y^2 + \sin\theta\cos\theta(\hat{F}_z\hat{F}_y + \hat{F}_y\hat{F}_z). \end{aligned} \tag{11}$$

and neglected the terms oscillating at high frequency

$$\begin{aligned} \cos(\Omega/2\delta\omega\sin(\delta\omega t)) &= J_0(\Omega/2\delta\omega) + 2\sum_{n=1}^{\infty} J_{2n}(\Omega/2\delta\omega)\cos(2n(\delta\omega t)) \\ &\approx J_0(\Omega/2\delta\omega) \\ \sin(\Omega/2\delta\omega\sin(\delta\omega t)) &= 2\sum_{n=0}^{\infty} J_{2n+1}(\Omega/2\delta\omega)\sin((2n+1)(\delta\omega t)) \approx 0, \end{aligned} \tag{12}$$

(verify how large $\delta\omega$ needs to be for this approximation to be valid)

In analogy to solid state stuff we introduce a new Fourier based spectroscopy technique that we use to measure the spin dependent energy-momentum dispersion bands of the system. With the addition of a one dimensional optical lattice, this work opens the ground for measurements of the Hofstadter butterfly spectrum.

Fixes:

- Write frequencies as ω_L and $\omega_L+\Delta\omega\pm\delta\omega$. Is there too many δ symbols, confusing?
- Call J_0 the zeroth order Bessel functions of the first kind.
- don't say modulation or multiple frequencies, just say we amplitude modulate by using
- no effective model, say the floquet Hamiltonian takes de form
- mention 2 paths, aka Molmer?
- say something about spin one paper?

Corrections of the effective Hamiltonian are of the order $1/\delta\omega$.